AIAA JOURNAL
Vol. 44, No. 10, October 2006

Comparison of Eddy-Viscosity Turbulence Models in Flows with Adverse Pressure Gradient

Alan Celić* and Ernst H. Hirschel†
Universität Stuttgart, 70550 Stuttgart, Germany

DOI: 10.2514/1.14902

Results of computations of aerodynamic flows with attached and separated boundary layers with adverse pressure gradients are presented. The objective is to compare the predictive accuracy of 11 eddy-viscosity turbulence models frequently employed for computing aeronautical flows. The turbulence models considered are the algebraic model of Baldwin and Lomax; the one-equation model of Spalart and Allmaras along with two additional variants of it; six different k, ω models; and the nonlinear eddy-viscosity model of Wallin and Johansson. Starting with a boundary-layer flow with a nominally zero pressure gradient, flows with a successively increased adverse pressure gradient are investigated. Computational results are compared with each other and to experimental data. It is found that the agreement between computational and experimental results varies between the turbulence models also for the simpler flow cases. Predictive accuracy obtained with a given model for a given flow case varies between the different flow variables evaluated. The "best" turbulence model changes from flow case to flow case. Models using transport equations for the eddy viscosity (or a related quantity) typically show better response to a pressure gradient than the algebraic Baldwin–Lomax model. However, no general conclusion on which model to use for adverse-pressure-gradient flows is drawn.

Nomenclature

a_1 = Bradshaw's parameter, 0.30
c = airfoil chord length
c_D = global drag coefficient
c_L = global lift coefficient
c_M = global moment coefficient
c_f = skin-friction coefficient, $\tau_w/(0.5\rho_r U_r^2)$
c_p = pressure coefficient, $(p - p_r)/(0.5\rho_r U_r^2)$
D = cylinder diameter
k = turbulent kinetic energy
L = length of the flat plate
M_r = reference Mach number
p = static pressure
p_r = reference static pressure
Re_r = reference Reynolds number
Re_θ = Reynolds number based on boundary-layer momentum thickness
S_{ij} = mean strain-rate tensor, $(1/2)(\partial u_j/\partial x_i + \partial u_i/\partial x_j)$
T_η = Kolmogorov's turbulence time scale
U_e = velocity at the boundary-layer edge
U_r = reference velocity
u = mean velocity parallel to the wall
u_i = components of the mean velocity vector
u_τ = friction velocity, $\sqrt{\tau_w/\rho}$
u^+ = sublayer-scaled velocity, u/u_τ
$-\overline{u'v'}$ = Reynolds shear stress per unit density
$-\overline{u_i'u_j'}$ = Reynolds stress tensor per unit density
x_j = Cartesian coordinates
y = distance normal to the wall
y^+ = sublayer-scaled distance normal to the wall, yu_τ/ν
δ = boundary-layer thickness
δ^* = displacement thickness, $\int_0^\delta (1 - u/U_e)\,\mathrm{d}y$
ϵ = turbulent dissipation rate per unit mass
θ = momentum thickness, $\int_0^\delta (u/U_e)(1 - u/U_e)\,\mathrm{d}y$
κ = Karman's constant, 0.41
μ = dynamic viscosity
μ_t = dynamic eddy viscosity
ρ_r = reference density
τ_w = wall shear stress
Ω_{ij} = mean rotation tensor, $(1/2)(\partial u_j/\partial x_i - \partial u_i/\partial x_j)$
ω = specific turbulent dissipation rate per unit mass, $\omega \propto \epsilon/k$

Subscript

m = maximum value in a profile taken normal to the wall

Introduction

ADVERSE-PRESSURE-GRADIENT flows are frequently encountered in engineering applications. Fast and accurate computations of such flows are therefore demanded by engineers in a wide variety of technical fields, e.g., in aircraft design. In most cases, computational predictions for such flows are obtained by solving the Reynolds-averaged Navier–Stokes equations in combination with eddy-viscosity turbulence models. Assessment of the predictive accuracy of turbulence models for adverse-pressure-gradient flows is therefore of general interest, and numerous studies have been undertaken in the past.

In the Air Force Office of Scientific Research (AFOSR) Stanford conferences [1,2] it was found that turbulence models at that time had difficulties in accurately predicting adverse-pressure-gradient flows. A direct successor of the Stanford conferences was the collaborative testing of turbulence models (CTTM) [3]. Its final report states that "the quality of results obtained seems to be much more closely correlated with the competence of the modeler/modeling group, the personnel available to do the actual running of test cases, and the adequacy of the computer program, than with the intrinsic quality of the turbulence model." The CTTM also revealed that a large scatter in computational results is obtained from different implementations of a single turbulence model, even for a simple flow like the flat-plate boundary layer.

The two European initiatives European Initiative on Validation of CFD Codes (EUROVAL) [4] and European Computational Aerodynamics Research Project (ECARP) [5] also address

Received 2 December 2004; revision received 13 February 2006; accepted for publication 29 May 2006.

*Research Engineer, Institut für Aero- und Gasdynamik, Pfaffenwaldring 21; alan.celic@googlemail.com.
†Professor, Institut für Aero- und Gasdynamik, Pfaffenwaldring 21; E.H. Hirschel@t-online.de. Senior Member AIAA.

predictive accuracy of turbulence models. In ECARP, a rating of the predictive capabilities of turbulence models is given for over 30 models. Only one model, the model proposed by Johnson and King [6], achieved "very good (reliable)" predictive accuracy for statistically two-dimensional separated flows. Fifty percent of the models yielded "poor" or "very poor" accuracy.

Recent development of promising turbulence models motivated the investigation of the predictive accuracy of some of these models for the computation of adverse-pressure-gradient flows with and without separation. Popular turbulence models that are in wide use are also included in the study to investigate the progress in turbulence modeling. All models are implemented in the same computer program, and the models' equations are solved with the same numerical method. This ensures that variances between results obtained with different models are due only to differences in turbulence modeling.

Four different flow cases are investigated in which the pressure gradient is increased from one flow case to the next. The predictive accuracy of the models is rated, and an attempt is made to judge which model is best suited for which flow class. Concerning computational results for the separated flows, special attention is paid to the prediction of the separation zone.

Numerical Method

Flow computations for this study have been performed with the FLOWer code developed at the Deutsches Zentrum für Luft- und Raumfahrt (DLR), Germany. Over recent years, FLOWer has become an important flow-analysis tool in the European aircraft industry [7]. It solves the three-dimensional unsteady and compressible Reynolds-averaged Navier–Stokes equations (RANS) in integral form on structured multiblock grids. For the solution of the mean-flow equations, a second-order central space discretization augmented by a blend of second- and fourth-order artificial damping terms is used. The explicit artificial damping terms prevent odd–even decoupling and damp spurious oscillations and allow for sharp shock resolution. For the time integration, an explicit five-stage Runge–Kutta scheme with optimized damping properties for multigrid methods is employed. Convergence to steady state is accelerated by means of local time stepping, implicit residual smoothing, full multigrid, and local preconditioning for low Mach numbers. The latter also insures high numerical accuracy when the Mach number becomes very low. This is an important issue when computing separated aerodynamic flows because in the separation region the fluid is typically moving at low Mach numbers even if the freestream Mach number is high. In addition, separated aerodynamic flows are encountered frequently in high-lift configurations of aircraft flying at low Mach numbers. Moreover, boundary-layer data for incompressible flows are more common, and probably more reliable, than measurements in compressible flows, and so testing of turbulence models, even for aeronautical purposes, should begin with the former. FLOWer is able to accurately compute high- and low-Mach number flows.

Convection terms of the transport-equation models are discretized by a first-order upwind scheme. Time integration is performed using a point-implicit scheme in which destructive source terms are treated implicitly and all remaining terms are treated explicitly. Note that using a first-order scheme for the convection terms in the model equations is deemed to be sufficiently accurate because the effect of the numerical scheme used for the convection terms in the turbulence model has no major effect on the flow solution. This is also observed, e.g., by Roache [8]. The benefit of using a first-order scheme is that it stabilizes the numerical solution.

A detailed presentation of the numerical algorithms used in FLOWer can be found in [9–12].

To verify grid convergence of the computational results obtained for the present study and to assess the influence of discretization errors on the flow solution, grid convergence studies for each flow case using at minimum three different grids were conducted. The ratio of grid spacings between different grids was two, i.e., starting from a fine grid, coarser grids were obtained by successively halving the number of grid cells in each coordinate direction. Generalized Richardson extrapolation was performed to estimate asymptotic values of the flow variables. The computational results discussed below were obtained either on the coarse or medium grids and were typically between 1 and 2% of the asymptotic value depending on the flow case, the flow variable, and the turbulence model considered.

Table 1 Turbulence models investigated

Model	Reference
Baldwin–Lomax	[13]
k, ω 1988 by Wilcox	[19]
k, ω 1998 by Wilcox	[15]
k, ω SST by Menter	[26]
k, ω SST modified	[30]
k, ω TNT by Kok	[20]
k, ω LLR by Rung and Thiele	[18]
EARSM of Wallin and Johansson	[14]
Spalart–Allmaras	[24]
Edwards–Chandra	[22]
SALSA by Rung et al.	[23]

Models Investigated

In the present study we mainly focus on transport-equation models. (For the sake of brevity, we denote eddy-viscosity transport models simply by "transport-equation models" because no Reynolds-stress transport models are considered in this work.) These models enjoy a large popularity in today's computational fluid-dynamics applications and constitute the aircraft industry's "work horses."

A total of 11 different turbulence models are considered (see Table 1). They range from the algebraic Baldwin–Lomax model over the Spalart–Allmaras, Edwards–Chandra, and strain-adaptive linear Spalart–Allmaras (SALSA) one-equation models to five different k, ω two-equation models. In addition, the nonlinear explicit algebraic Reynolds-stress model (EARSM) proposed by Wallin and Johansson [14] is also investigated.

We have not included a classical k, ϵ model in our study because its deficiencies for predicting aerodynamic flows with adverse pressure gradients have been shown by others [15–17]. In addition, the k, ϵ model is not as commonly used for aeronautical applications as most of the models considered in the present work.

The Johnson–King model is not included in our comparison, although it gave good results in previous studies. The reason is simply that the model is tailored for computations of two-dimensional flows and is rarely implemented in CFD codes that are used to compute three-dimensional flows around complete aircraft like FLOWer. (There exist extensions of the Johnson–King model to three-dimensional flows, but these models do not offer the high-predictive performance of the original model, see [5].)

All models are applied in the version proposed by the referenced authors unless otherwise noted. The reader may refer to the cited literature for details of the models. Comments are made in the following about models which are believed to be less known and models that are implemented differently in FLOWer than proposed in the referenced literature. Note, not all models were implemented into FLOWer by the authors themselves. For example, the k, ω linear realizable (LLR) and the SALSA models have been implemented by the model developers at the Technical University of Berlin. In particular, the k, ω LLR model in FLOWer is slightly different than the model presented in [18].

The 1998 version of Wilcox's k, ω model [15] is based on the 1988 model [19]. In the newer model a so-called cross-diffusion term is used to modify a closure coefficient in the equation for k. The main objective is to resolve the round-jet/plane-jet anomaly of the 1988 model and to reduce its sensitivity in free shear layers to the freestream value of ω.

Similarly, the k, ω turbulent/nonturbulent (TNT) model of Kok [20] also builds on Wilcox's 1988 k, ω model and uses a cross-diffusion term to yield results that are independent of the specified

freestream value of ω. However, unlike in the 1998 Wilcox model, cross diffusion is not used to modify model coefficients. Instead, the cross-diffusion term is added to the transport equation for ω. In addition, diffusion coefficients are proposed such that a correct model behavior is recovered at turbulent/nonturbulent interfaces.

The k, ω LLR model of Rung and Thiele [18] is closely related to the realizable k, ϵ model developed by Shih et al. [21]. The rationale behind these models is to explicitly secure realizability, i.e., $-\overline{u_i' u_i'} \leq 0$ and $(\overline{u_i'^2})(\overline{u_j'^2}) \geq (\overline{u_i' u_j'})^2$. Rung and Thiele reformulated the model of Shih et al. in terms of ω and applied further modifications. These comprise low-Reynolds-number damping functions to achieve the correct asymptotic near-wall behavior of the turbulent kinetic energy ($k \propto y^2$). The equations of the resulting k, ω LLR model implemented in FLOWer and applied for the present study read as follows:

$$\mu_t = c_\mu \rho \frac{k}{0.09\omega}$$

$$\frac{\partial \rho k}{\partial t} + \frac{\partial \rho k u_j}{\partial x_j} = -\rho \overline{u_i' u_j'} \frac{\partial u_i}{\partial x_j} - \beta_k \rho k \omega + \frac{\partial}{\partial x_j}\left[\left(\mu + \frac{\mu_t}{2}\right)\frac{\partial k}{\partial x_j}\right]$$

$$\frac{\partial \rho \omega}{\partial t} + \frac{\partial \rho \omega u_j}{\partial x_j} = \alpha_\omega \frac{\omega}{k}(-\rho \overline{u_i' u_j'})\frac{\partial u_i}{\partial x_j} - \beta_\omega \rho \omega^2 + \frac{\partial}{\partial x_j}\left[\left(\mu + \frac{\mu_t}{2}\right)\frac{\partial \omega}{\partial x_j}\right]$$

Auxiliary relations for the eddy viscosity are as follows:

$$c_\mu = f_\mu c_\mu^*, \qquad f_\mu = \frac{1/80 + R_\mu}{1 + R_\mu}$$

$$c_\mu^* = \max\left[0.04, \min\left(\frac{1}{(b_0 + A_s)\tilde{U}}, 0.12\right)\right]$$

$$R_\mu = \left(\frac{R_t}{70}\right)^\alpha, \qquad R_t = \frac{k}{0.09\omega\nu}$$

$$\alpha = \frac{1}{2} + 1.6\left[3\left(\frac{R_t}{150}\right)^2 + 2\left(\frac{R_t}{150}\right)^3\right]$$

$$b_0 = \max\left(\frac{a_0}{\tilde{U}}, \frac{181}{140 + [S/(0.09\omega)]^2}\right)$$

$$A_s = 3\cos\left[\frac{1}{2}\arccos\left(\sqrt{48}\frac{III}{S}\right)\right]$$

$$\tilde{U} = \frac{\sqrt{(1/2)(\Omega^2 + S^2)}}{0.09\omega}$$

$$a_0 = 8.0 - 4.1\tanh\left(\frac{S}{1.8 \cdot 0.09\omega}\right)$$

$$S = \sqrt{2S_{ij}S_{ij}}, \qquad \Omega = \sqrt{2\Omega_{ij}\Omega_{ij}}, \qquad III = S_{ij}S_{jk}S_{ki}$$

Auxiliary relations for the k-destruction term are as follows:

$$\beta_k = 0.09\frac{0.83/3 + R_k}{1 + R_k}$$

$$R_k = A^*\left(\frac{R_t}{100}\right)^{2.5} + (1 - A^*)\sqrt{\frac{R_t}{100}}$$

$$A^* = \tanh\left(4\sqrt{\frac{R_t}{100}}\right)$$

Auxiliary relations for the ω-production term are as follows:

$$\alpha_\omega = \frac{5}{9}(1 - f_\beta) + \frac{5}{9}\frac{0.09}{c_\mu^* f_\beta}$$

$$f_\beta = \frac{1/80 + R_{tf}}{1 + R_{tf}}, \qquad R_{tf} = \left(\frac{R_t}{10,000}\right)^2$$

The auxiliary relation for the ω-destruction term is as follows:

$$\beta_\omega = 0.09\left(\frac{1.83}{1 + \sqrt{\mu c_\mu/(\mu + \mu_t)}}\right)$$

The model proposed by Edwards and Chandra [22] as well as the SALSA model suggested by Rung et al. [23] are both based on the one-equation model of Spalart and Allmaras [24]. In the Edwards–Chandra model the production term and the near-wall parameter of the original Spalart–Allmaras model are reformulated to improve its numerical properties without affecting the predictive behavior. In the SALSA model the level of Reynolds stresses is reduced in regions of excessive strains by assuming a constant maximum value of the ratio a_1 between Reynolds shear stress and turbulent kinetic energy. Bradshaw et al. [25] chose from experiments $a_1 = -\overline{u'v'}/(2k) = 0.15$. Later workers have often used the symbol a_1 for twice this quantity, and so the numerical value is about 0.30. The modified k, ω SST model also builds on this assumption ($a_1 = 0.30$) whereas the SST model in [26] uses $a_1 = 0.31$. Note that different versions of the SST model exist using different values for the closure coefficients including a_1. However, the version published in [26] is recommended by Menter and is used in the current work. Numerical results showed sensitivity to the value of a_1 used in the SST model. However, this is not discussed further in the current work.

The Wallin–Johansson [14] model applies a nonlinear constitutive relation for computing the eddy viscosity consisting of functionals of S_{ij} and Ω_{ij}. It also relies on the Wilcox 1988 model for the computation of k and ω, which are used to scale the terms in the constitutive relation. The main advantage of this model over the linear ones is its ability to predict anisotropy of normal Reynolds stresses.

An attempt was made to further improve predictions of the k, ω SST model. Two simple modifications of the SST model of Menter [26] were implemented for this purpose.

Eddy Viscosity in the Viscous Sublayer

The original k, ω SST model of Menter sets the eddy viscosity in the viscous sublayer proportional to k/ω. It can be shown that this gives the following asymptotic sublayer behavior:

$$\mu_t \propto y^n \quad \text{for } y \to 0$$

with $n \approx 5.23$. However, the physically correct value of n is $n \approx 3$ (see, e.g., Wilcox [15]). Hence, a functional dependence of μ_t on k and ω that yields an exponent closer to the theoretical value of 3 in the viscous sublayer would be more appropriate. This can be achieved as follows.

In the viscous sublayer the turbulent motion is strongly affected by the presence of the solid surface; the turbulent eddies decrease in size approaching the wall. Because small scale turbulent motions are diffused and dissipated by viscosity, it is therefore appropriate to base the characteristic turbulence time scale in the viscous sublayer on the viscosity and the turbulence dissipation:

$$T_\eta \propto \sqrt{\frac{\nu}{\epsilon}} \propto \sqrt{\frac{\nu}{k\omega}}$$

Because the eddy viscosity can be written as a product of k and a time scale, it seems to be reasonable to use T_η to compute the eddy viscosity in the viscous sublayer. For this purpose the following expressions were implemented into the SST model:

$$\mu_t = (S_L \rho \nu)^{F_3} \left(\frac{a_1 \rho k}{\max(a_1 \omega; \Omega F_2)} \right)^{1-F_3}$$

$$F_3 = \frac{1}{2} \tanh(\arg^4)$$

$$\arg = \max\left[1 - \frac{k/\omega}{\sqrt{S_L \nu k/\omega}}, 0 \right], \qquad S_L = 2$$

F_3 ensures a smooth transition from the sublayer expression $\mu_t = \sqrt{S_L k \nu/\omega}$ to the standard SST formulation for the eddy viscosity. This reformulation of the eddy viscosity in terms of T_η yields $n \approx 2.62$ for the asymptotic behavior approaching the wall.

Reducing ω in the Logarithmic Region

Analysis of eddy-viscosity profiles in a flat-plate boundary layer revealed that μ_t computed with the original k, ω SST model is lower than μ_t inferred from the experiment for $40 \le y^+ \le 200$. To investigate to what extent these differences do have an influence on the computed velocity profile the eddy viscosity was increased in the region of interest. For this purpose a local damping of ω around $y^+ = 75$ was introduced, which was achieved by increasing the destruction term in the ω equation. In particular, the destruction coefficient β_1 of the SST model was modified as follows:

$$\beta_1 = \frac{1}{(1 - 1.3F_4)} \frac{3}{40}$$

$$F_4 = \max\left\{ \exp\left[-\frac{1}{2} \left(\frac{75 - y^+}{85} \right)^2 \right] - 0.7, 0 \right\}$$

This is an ad-hoc modification to improve predictions of the eddy-viscosity profile in a zero pressure gradient boundary layer. There is no deeper physical reasoning besides matching the behavior between computed eddy viscosity and the eddy viscosity inferred from measured data for a flat-plate boundary layer.

As noted above, the older (1988) version of the k, ω model by Wilcox yields results that depend on the value specified for ω at the far field. However, Menter [27] showed that for boundary-layer flows the dependency is insignificant if $\omega > (40/3)(u_\tau^2/U_e \delta^*)$ at the boundary-layer edge. For the present study, ω at the far-field boundaries was set using following relations:

$$\omega = \frac{\rho_r k}{\mu_t}, \qquad k = \frac{3}{2}(5 \times 10^{-3} U_r)^2, \qquad \mu_t = 0.001\mu \quad (1)$$

Evaluating Menter's condition using the results obtained in the present study showed that the condition was satisfied by applying Eq. (1). In addition, lowering k (and, hence, ω) by 1 order of magnitude had no effect on the solutions. Note that Eq. (1) was used for all k, ω models considered.

Test Cases Selected

The flow cases investigated have, on the one hand, a simple geometry to simplify grid generation, to exclude numerical errors associated with extremely skewed grid cells, and to be easily able to study grid convergence effects by simply doubling the number of grid points. On the other hand, they are well suited for validation purposes because for each flow case extensive experimental data are available and each flow case offers the necessary physical complexity. Table 2 gives an overview of the flow cases considered including the basic flow parameters which were specified for the computations. A closer description of the investigated flow is given in the corresponding section.

Table 2 Test cases and basic flow parameters

Test case	Name	M_r	Re_r	T_r, K
Boundary layer with $dp/dx = 0$	FPBL	0.03	4.47×10^6	296.4
Nonequilibrium boundary layer with $dp/dx > 0$	BS0	0.09	2.8×10^5	291.1
Nonequilibrium boundary layer with $dp/dx > 0$ and separation	CS0	0.09	2.8×10^5	291.1
Separated flow around airfoil A	AAA	0.15	2×10^6	294.4

Results and Discussion

Flat Plate Case

A flat-plate boundary-layer (FPBL) flow with zero pressure gradient is considered to investigate the models' predictions for the law of the wall. An accurate prediction of the law of the wall is an important requirement for turbulence models applied for the computation of aerodynamic flows.

Menter [17] as well as Bardina et al. [16] performed computations of a flat plate boundary layer using different turbulence models including the k, ω 1988 model and the k, ω SST model. They found that all models investigated in their work gave good results for the flat-plate flow. Wilcox [15] also tested a variety of models for the prediction of flat-plate boundary layers. He found that the k, ω 1998 model gave accurate predictions of skin friction.

Accurate experiments of such a flow were performed by DeGraaff and Eaton [28] and are used here for validation of the models. The advantage of DeGraaff's and Eaton's data over earlier measurements is that the first measurement point of the boundary-layer profiles is located very close to the wall, well within the viscous sublayer, so that model predictions of the sublayer can be checked in detail. In the experiment, the boundary-layer profiles were evaluated at a downstream position corresponding to $Re_\theta = 2900$; the freestream velocity was $U_r = 9.83$ m/s. In the computation, to resemble approximately the value for U_r, $M_r = 0.02848$ and $Re_r = 6.4 \times 10^5$ m^{-1} were specified. Transition was prescribed at $x/L = 0.04$ that yields $Re_\theta = 2900$ at approximately 40% of the plate length. Transition in this context means that productive source terms in the turbulence-model equations are set to zero upstream of the transition location thereby ensuring negligible μ_t and, in turn, a laminar flow solution. The computational grid was designed so that $y^+ < 1$ at the first grid point above the wall.

Computational results for this flow show that the k, ω 1988 and k, ω 1998 models underpredict the u^+ profiles in the boundary layer compared with measurements (Fig. 1). All other models yield u^+ that is in close agreement with the experimental data, although the original k, ω SST model and the k, ω TNT model show a tendency to yield a value for κ that is too low (i.e., the slope of u^+ is too high in the log region).

Variations among the results obtained with different models are more pronounced for c_f than for u^+ (Table 3). The computational results for c_f deviate between roughly 1 and 11% from the experimental value. The best agreement of c_f with the experimental result is obtained with the modified k, ω SST model; the k, ω 1988 model yields the largest deviation.

Driver–Johnston Cylinder

The next flow cases considered are turbulent boundary layers with a strong adverse pressure gradient that were experimentally investigated by Driver and Johnston [29]. In these flows, an axisymmetric boundary layer developed in the axial direction on a circular cylinder; the cylinder was lengthwise mounted along the centerline of the wind tunnel (Fig. 2). Note that Driver's and Johnston's main interest was in the case where the cylinder rotated

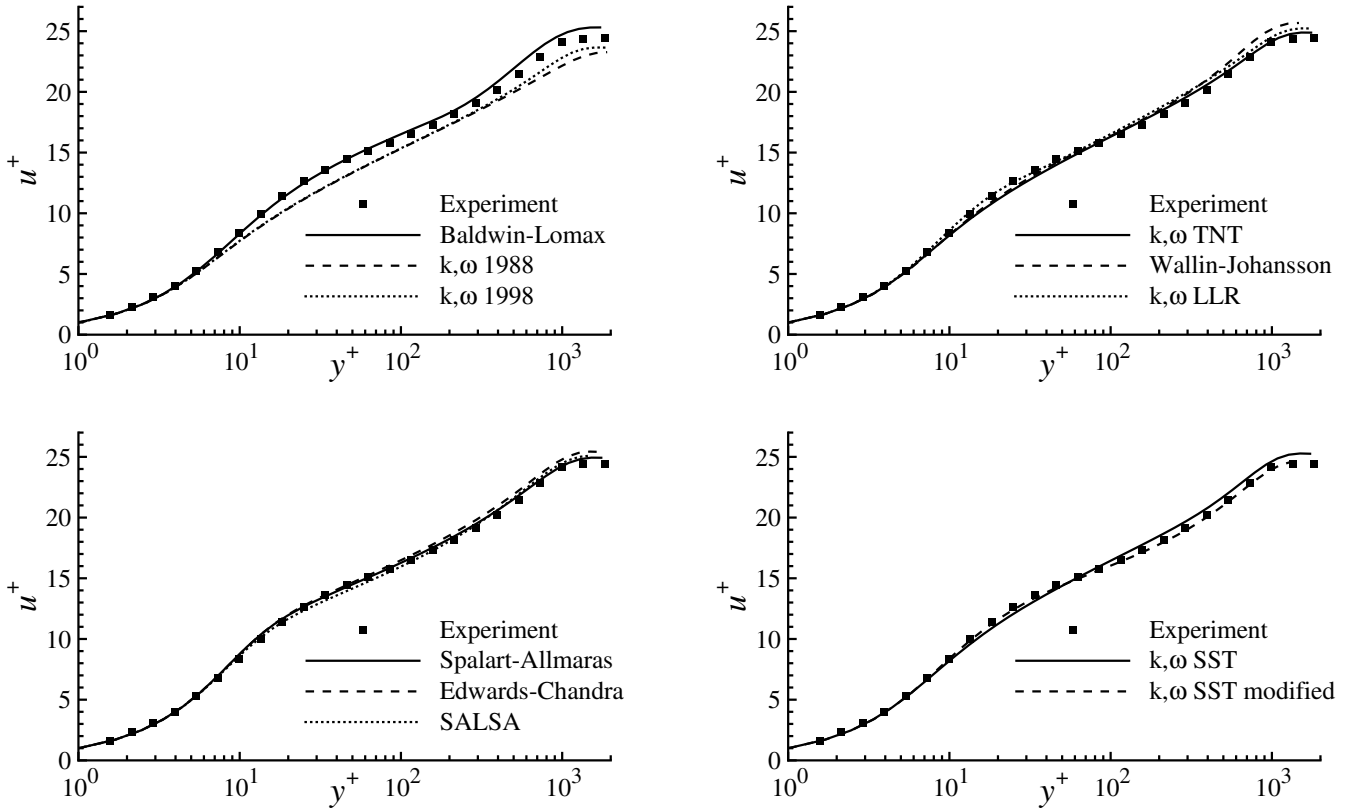

Fig. 1 Velocity profiles for flat-plate boundary layer (case FPBL).

giving a three-dimensional boundary layer. The results used here were for zero rotation.

An adverse pressure gradient was imposed on the cylinder by diverging all four wind-tunnel walls. Boundary-layer suction at the tunnel walls was used to control the level of pressure gradient along the cylinder. Two cases with a strong a adverse pressure gradient resulting in nonequilibrium flows were studied: case BS0 without separation of the boundary layer at the cylinder and case CS0 with separation. Driver's and Johnston's extensive experimental data for these flow cases include wall pressure and wall shear-stress distributions, mean velocity profiles, and Reynolds stresses. The data are highly accurate and self-consistent and form an excellent basis to assess the predictive performance of turbulence models, and several researchers have computed this flow for testing turbulence models [15,26,16]. In these studies, results obtained from different models varied, in particular, for the separated case CS0.

In our computations, measured profiles were prescribed at the inflow boundary; convective outflow conditions (i.e., zero gradients) were specified at the outflow boundary. At the cylinder wall, the usual no-slip condition was applied. The upper boundary was identical to an inviscid streamline extracted from the experimental data. Along this boundary, the velocity vectors were forced to be tangential to the boundary resulting in a so-called Euler-wall condition. This follows closely the procedure proposed by Menter [17] and proved to be a valid method for indirectly specifying longitudinal pressure gradients in boundary layers in the framework of computations of the full Navier–Stokes equations. As a result of the inviscid-streamline procedure, an internal flow is obtained. Hence, the pressure at the downstream boundary had to be iteratively adapted during the computations to achieve a smooth c_p distribution at the inflow region.

The Reynolds number based on the cylinder diameter was $Re_r = 2.8 \cdot 10^5$, and the Mach number was specified to be $M_r = 0.08772$, which corresponds to $U_r = 30$ m/s in the experiments.

Table 3 Local c_f at $Re_\theta = 2900$ (flat plate)

Source	$c_f \times 10^3$	Δ, %
Experiment	3.362	——
k, ω SST modified	3.325	−1.1
k, ω TNT	3.264	−2.9
Spalart–Allmaras	3.250	−3.3
SALSA	3.209	−4.6
k, ω LLR	3.179	−5.4
k, ω SST	3.168	−5.8
Baldwin–Lomax	3.147	−6.4
Edwards–Chandra	3.132	−6.8
k, ω 1998	3.613	+7.5
Wallin–Johansson	3.074	−8.6
k, ω 1988	3.726	+10.8

Adverse-Pressure-Gradient Boundary Layer without Separation

Figure 3a shows pressure and skin-friction distributions along the cylinder surface. The graphs of the pressure distributions obtained with different models lie very close to each other up to $x \approx 0$. Downstream of this point some differences among the pressure distributions are seen: The Baldwin–Lomax model yields the highest

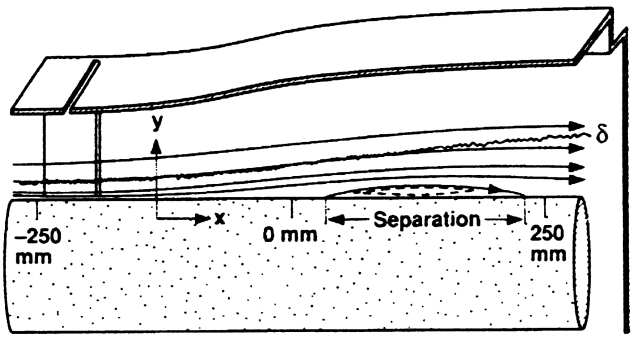

Fig. 2 Schematic of Driver's and Johnston's cylinder flow (courtesy of David Driver, NASA, Ames Research Center; used with permission).

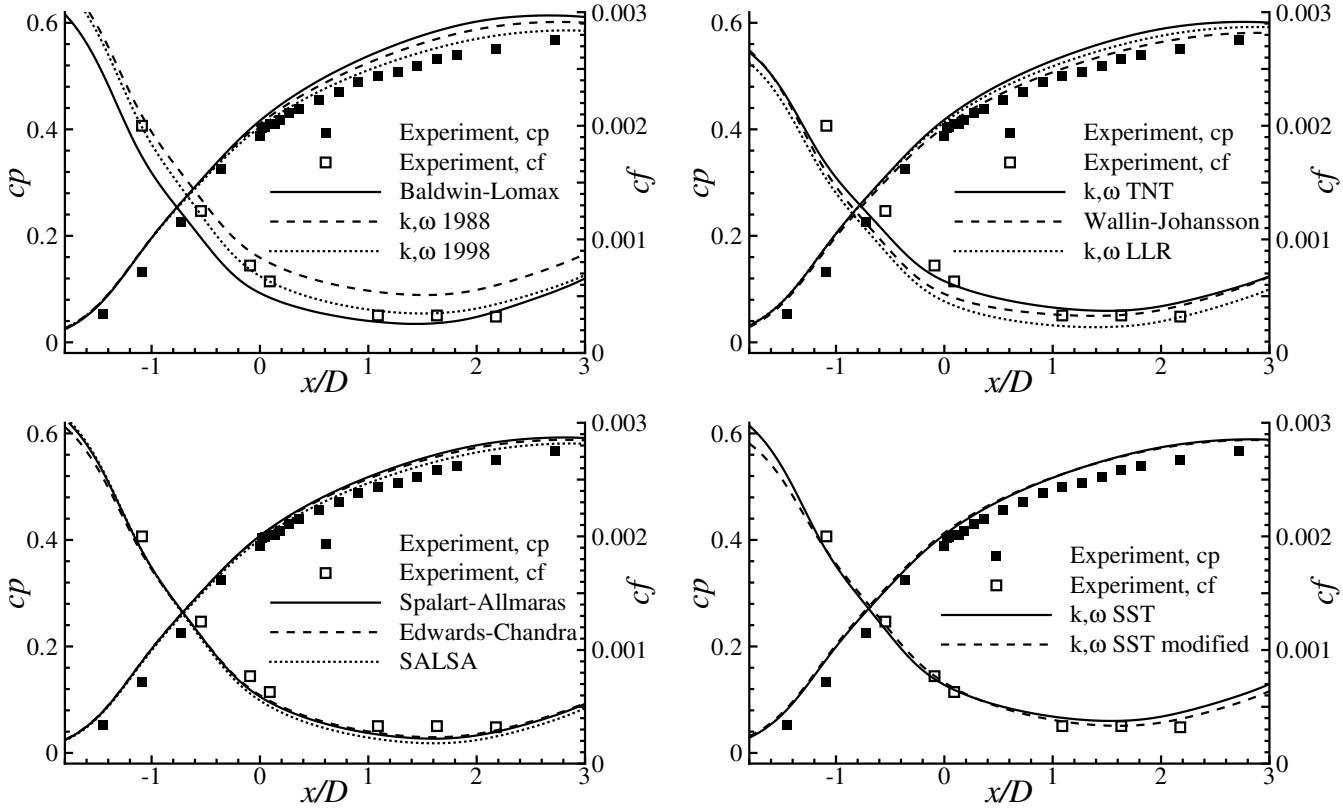

a) Case BS0 (no separation)

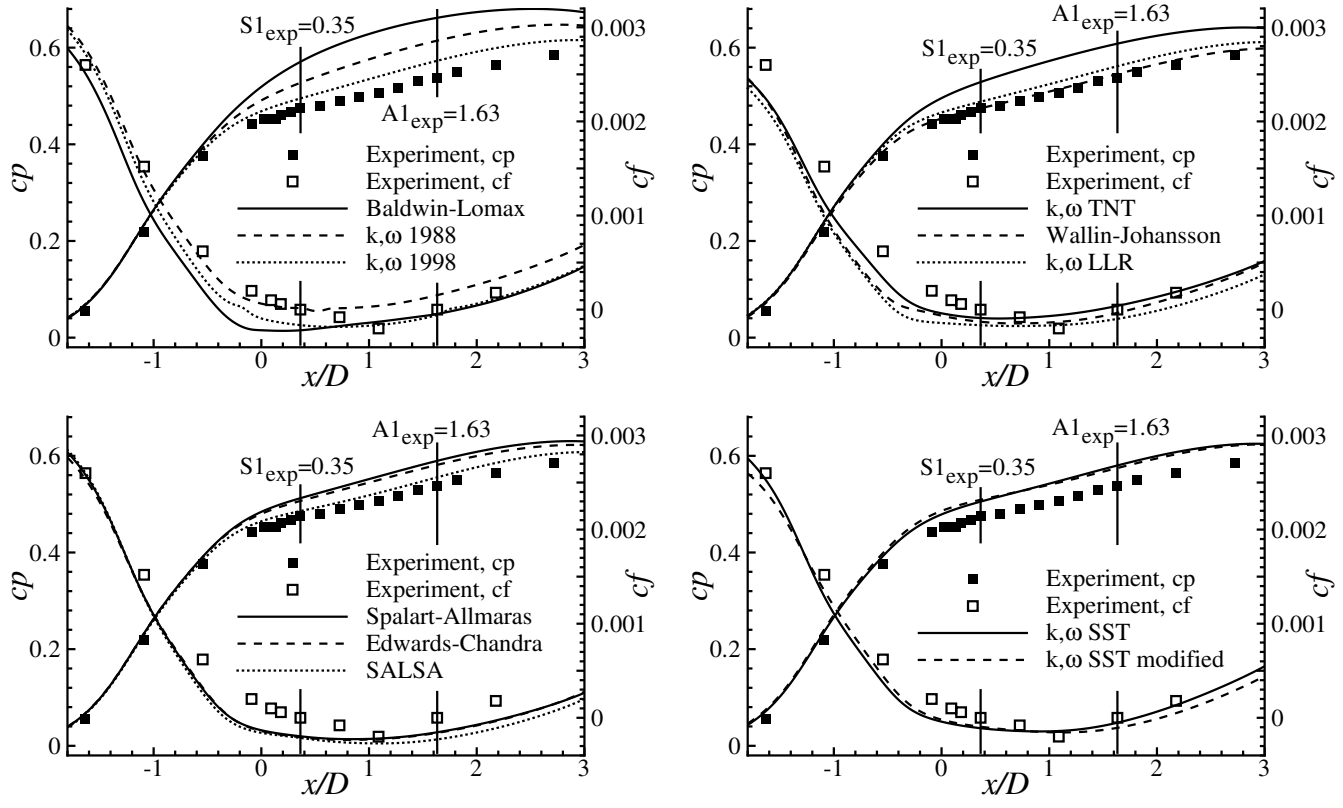

b) Case CS0 (with separation)

Fig. 3 Pressure and skin-friction distributions for turbulent boundary layers with strong streamwise pressure gradient.

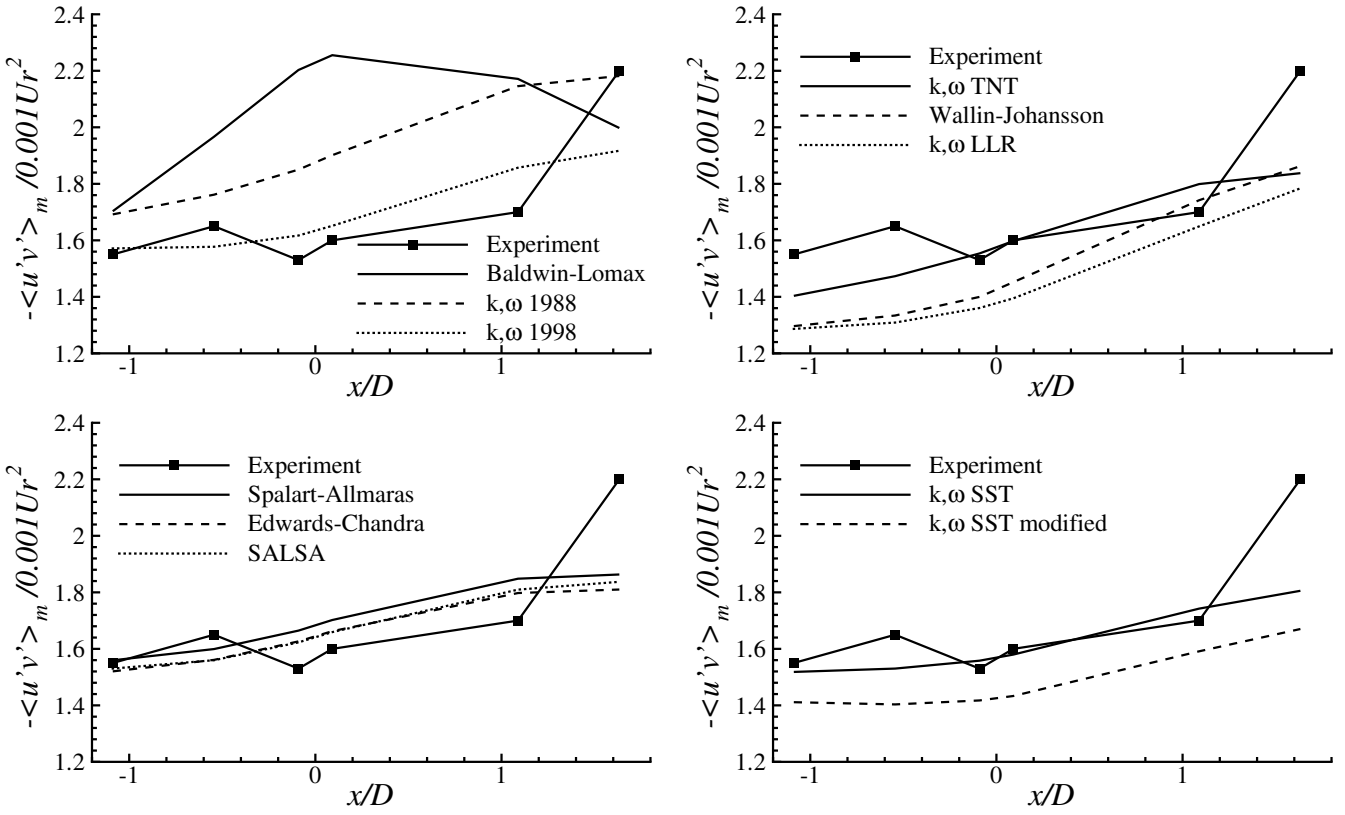

Fig. 4 Streamwise development of $-\overline{u'v'}_m$ for case BS0.

surface-pressure level whereas the SALSA model, the Wallin–Johansson model, and the 1998 Wilcox model predict the lowest pressure values and are therefore in closest agreement with the measurements.

Variations between the skin-friction distributions are somewhat larger than the small variations in c_p. In particular, the differences in c_f obtained from different k, ω models, e.g., the two Wilcox models, are larger than the differences in c_f computed with the different one-equation models. However, the 1998 k, ω model by Wilcox and the two k, ω SST models give the best results for c_f for this flow case.

Regarding streamwise development of maximum Reynolds shear stress, the Baldwin–Lomax model computes a $-\overline{u'v'}_m$ that is in rather poor agreement with the experimental data (Fig. 4). In particular, the overall maximum of $-\overline{u'v'}$ is predicted at $x = 0$, which is too far upstream. Downstream of this point, $-\overline{u'v'}_m$ decreases, which indicates that the Baldwin–Lomax model quickly responds to the change of pressure gradient. This behavior is not seen in the results obtained with the other models; they yield overall maxima of $-\overline{u'v'}$ further downstream at $x/D = 1.6$, as it is encountered in the measurements. These models are based on transport equations that do, to some extend, account for flow-history effects. Flow-history effects are believed to be the reason why in this flow Reynolds stresses do not immediately respond to changes in the pressure gradient.

Profiles of the mean velocity u at several different downstream positions have been also evaluated. However, the corresponding graphs are not shown in this paper for the sake of brevity, and the reader is referred to [30] for more details.

Rating System

To assess performance of the turbulence models, we use a rating system that is based on the differences between computed and measured values.

For each experimental data point shown in the figures, the absolute differences between the experimental data and the value predicted by a turbulence model were computed and normalized with a reference value. These normalized differences were summed up and divided by the number of data points N to obtain averaged normalized differences (AND). The following equation illustrates this procedure using c_p:

$$\text{AND} = 100\frac{1}{N}\sum_{i=1}^{N}\left|\frac{\left(c_p^{\text{exp}}\right)_i - \left(c_p^{\text{comp}}\right)_i}{\left(c_p^{\text{exp}}\right)_m}\right| [\%] \qquad (2)$$

Hence, AND is a measure of how well computational values of flow variables agree with the experimental ones. As indicated in Eq. (2), the maximum experimental value was typically used as a reference value to compute averaged normalized differences. Normalizing with the corresponding maximum values gives more optimistic results for AND than using, for example, corresponding local values. Therefore, we define very poor predictive performance (denoted with $---$) if AND $> 12\%$ for a given model and flow variable. In contrast, very good agreement (denoted with $+++$) is defined if $0\% \leq \text{AND} \leq 2\%$, good agreement (denoted with $++$) is achieved if $2\% < \text{AND} \leq 4\%$, and so on.

The outlined method enables us to rate consistently predictions of the turbulence models. The ratings for case BS0 are summarized in Table 4. Note that instead of listing values for AND, we prefer to use

Table 4 Turbulence-model performance for case BS0

Model	c_p	c_f	$u(y)$	$-\overline{u'v'}_m$	$\sum$
k, ω 1998	2(++)	2(+++)	+++	+	14+
k, ω SST	2(+)	2(++)	+++	+	10+
Edwards–Chandra	2(++)	2(+)	+++	+	10+
Spalart–Allmaras	2(++)	2(+)	++	+	9+
k, ω SST modified	2(+)	2(++)	+++	−	8+
SALSA	2(++)	◯	++	+	5+
Wallin–Johansson	2(++)	2(−)	+++	−	5+
k, ω TNT	2(+)	◯	++	◯	4+
k, ω 1988	2(+)	◯	++	−−	1+
k, ω LLR	2(+)	2(−−)	+++	−−	1−
Baldwin–Lomax	◯	◯	◯	−−−	3−

Table 5 Symbols used to rate turbulence-model performance

Symbol	Meaning
+ + +	Very good agreement with measurements
++	Good agreement with measurements
+	Fair agreement with measurements
◯	Modest agreement with measurements
−	Weak agreement with measurements
−−	Poor agreement with measurements
− − −	Very poor agreement with measurements

symbols to make reading of the table more intuitive. The explanation of the rating symbols is summarized in Table 5.

From an engineering point of view, c_p and c_f are frequently more important than $u(y)$ or $-\overline{u'v'}(y)$. Therefore, ratings for c_p and c_f are weighted by a factor of 2, as indicated in Table 4. The last column in the table contains the sum of ratings given for each model.

We are aware that our rating system is more qualitative than purely quantitative. Experimental data are subject to uncertainties that may be greater than the differences in computational results. This holds, in principle, also for the experimental data used in the current work. Similarly, uncertainties in the computational results obtained may arise from boundary conditions, computational grids, and the numerical method. Judging absolute predictive performance of the turbulence models requires taking these uncertainties into account. In light of the high accuracy of the experimental data of, e.g., Driver and Johnston and the grid convergence tests performed for every flow case, we feel that the suggested rating system is a legitimate approach. In any case, our system is meant to give qualitative rather than absolute quantitative conclusions about the models' predictive performances. This approach indicates that Wilcox's k, ω 1998 model gives the best overall results for flow case BS0 (Table 4).

Adverse-Pressure-Gradient Boundary Layer with Separation

For case CS0, computed and measured geometries of the dividing streamlines of the recirculation zone are shown in Fig. 5. $S1_{exp}$ and $A1_{exp}$ denote the separation and reattachment points, respectively, determined form the experimental data.

The Baldwin–Lomax, the k, ω 1988, and the k, ω TNT models predict recirculation zones that are thinner than the one inferred from experimental data. In fact, the k, ω 1988 model yields the thinnest separation zone, and the corresponding dividing streamline is not visible in Fig. 5. All models except the k, ω 1988 model yield recirculation zones that extend further in the streamwise direction than in the experiment, i.e., the distance between S1 and A1 is larger in the computational results than in the experiment. This is also seen from the skin-friction distributions discussed hereafter. For the k, ω 1998 model, predictions are in good overall agreement with the experimental recirculation zone. The SALSA model predicts a larger recirculation zone compared with the experiment and with results obtained with the other one-equation models. Very good agreement between measured and computed data of flow topology is obtained with the original k, ω SST model; the modified SST model predicts a slightly larger separation zone than measured.

Regarding the surface-pressure distribution along the cylinder, all turbulence models yield results that are in close agreement with measurements up to $x/D \approx -0.4$ (Fig. 3b). Downstream of this point, however, variances are found between pressure distributions obtained with different models implying large differences in displacement thickness. Whereas most models overpredict surface pressure in this region, the model of Wallin and Johansson virtually duplicates experimental results. The Baldwin–Lomax model yields the poorest agreement of c_p with measurements; all other model predictions are in between these extrema.

In Fig. 3b, locations of boundary-layer separation and reattachment were defined at points where $c_f = 0$. In the experiment, c_f was measured independently from the velocity. However, the positions of S1 and A1 inferred from the streamfunction, i.e., from velocity, and those obtained from the c_f distribution were found to be almost identical, which indicates high consistency and accuracy of the experimental data.

Predictions of c_f obtained with the one-equation models are closer to each other than the predictions of the k, ω models. Wilcox's 1988 k, ω model yields $c_f = 0$ in close agreement with the experimental separation point. Furthermore, the model yields a skin-friction distribution that is close to measurements up to separation. However, it computes a very thin separation zone and predicts reattachment further upstream than measured. The SALSA model computes c_f values that are very close to the results obtained with the other one-equation models. Yet, it yields predictions for c_p that differ from the predictions obtained with the other one-equation models.

Concerning the results for c_p and c_f, the following conclusion is drawn: If a turbulence model yields c_p in good agreement with experimental data, it does not necessarily yield c_f in comparable agreement with the experiment. This is best recognized from results obtained with the SALSA model and the k, ω LLR model: These models yield c_p that is close to measurements whereas they predict c_f in weak agreement with the experiment (see Table 6 and Fig. 3b).

We now turn to the streamwise development of maximum Reynolds shear stress shown in Fig. 6. Compared with the experimental data, the Baldwin–Lomax model predicts the maximum of $-\overline{u'v'}$ further upstream, thus responding too quickly to the decrease in the pressure gradient. The other models yield results in better qualitative agreement with the experiment, and they predict the maximum of $-\overline{u'v'}$ further downstream than the

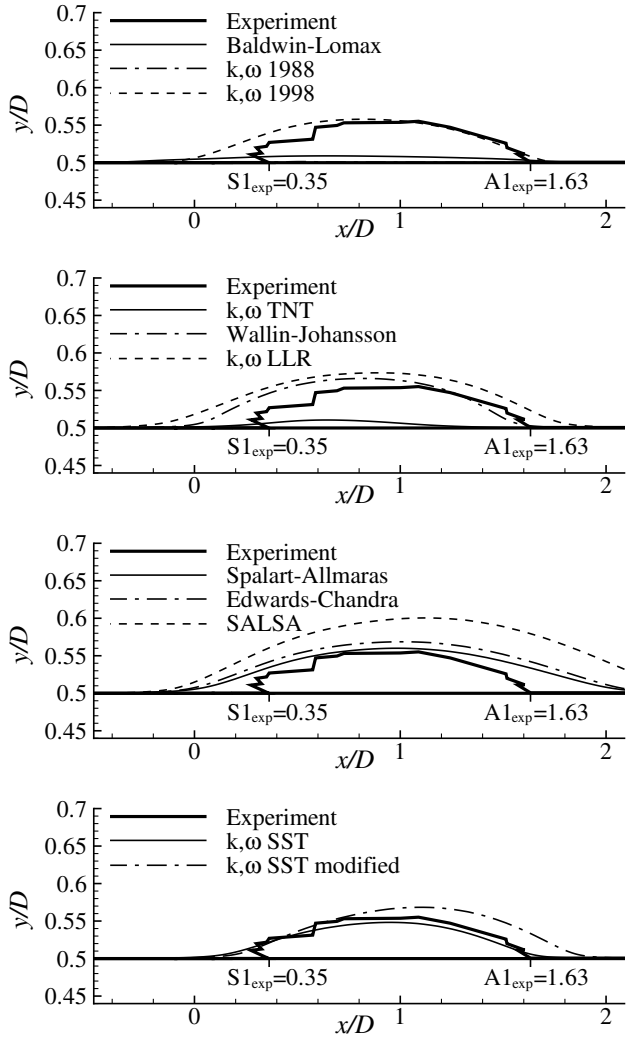

Fig. 5 Geometries of recirculation zones for case CS0; dividing streamlines are shown.

Table 6 Turbulence-model performance for case CS0

Model	c_p	c_f	Separation zone	$-\overline{u'v'}_m$	$\sum$	BS0 + CS0
Wallin–Johansson	2(+ + +)	◯	+	+	8+	10+
k, ω SST	2(+)	2(+)	+ + +	◯	7+	17+
k, ω SST modified	2(+)	2(+)	++	+	7+	15+
k, ω 1998	2(+)	◯	++	−	3+	17+
k, ω LLR	2(++)	2(−)	◯	+	3+	2+
Edwards–Chandra	2(+)	◯	+	−	2+	12+
SALSA	2(++)	2(−)	◯	−	1+	6+
Spalart–Allmaras	◯	◯	+	−	◯	9+
k, ω 1988	2(−)	2(+)	−−	− − −	5−	4−
k, ω TNT	2(−)	◯	−−	−	5−	1−
Baldwin–Lomax	2(− − −)	2(−)	− − −	− − −	14−	17−

Baldwin–Lomax model. This is attributed to the fact that all models except the Baldwin–Lomax model are based on transport equations. However, the transport-equation models also predict the maximum of $-\overline{u'v'}$ further upstream than found in the experiment. Downstream of reattachment A1 in the experiment ($x/D \geq 1.63$), all models yield $-\overline{u'v'}_m$ that is decreasing in the downstream direction. This is in contrast to the experimental results where a further increase of $-\overline{u'v'}_m$ in the streamwise direction is found. Up to $x/D = 1.1$, the modified k, ω SST model yields the best agreement of streamwise development of $-\overline{u'v'}_m$ with the experimental results. The general trend of increasing $-\overline{u'v'}_m$ is best reproduced by the Wallin–Johansson model and the k, ω LLR model.

The agreement of computational results and measured data for case CS0 is summarized in Table 6 in a similar manner as for case BS0. The only difference is that instead of comparing velocity profiles we rate the agreement of separation-zone geometries, i.e., the height of the separation region and locations of detachment and reattachment.

The last column of Table 6 contains the sum of the ratings for both cases BS0 and CS0. For case CS0, the best overall results yield the Wallin–Johansson model and the k, ω SST models.

Separated Airfoil Flow

The mildly separated flow around the Aerospatiale-A airfoil at a Reynolds number based on chord length of 2×10^6, a Mach number of 0.15, and an angle of attack of 13.3 deg was investigated (case AAA). Experiments were conducted at ONERA, and a complete database of the experimental results is available in [31]. In the experiments, transition at the lower surface was fixed with a trip at 30% of the chord length. On the upper side, free transition was allowed, and a laminar separation bubble, with turbulent reattachment at 0.12 chord length, was observed during the tests. A broad set of available experimental data including profiles of u and $-\overline{u'v'}$ in the boundary layers and in the near wake, boundary-layer thicknesses, skin-friction, and surface-pressure data make this flow case especially attractive for the validation of turbulence models for computing separated airfoil flows.

Hence, this flow case has been extensively used for turbulence-model testing in [5]. Significant scatter was found among results obtained with different turbulence models, with all model predictions being in rather weak agreement with experimental data. This flow case also served as a validation test case for large eddy simulations for aerodynamic applications, e.g., in [32].

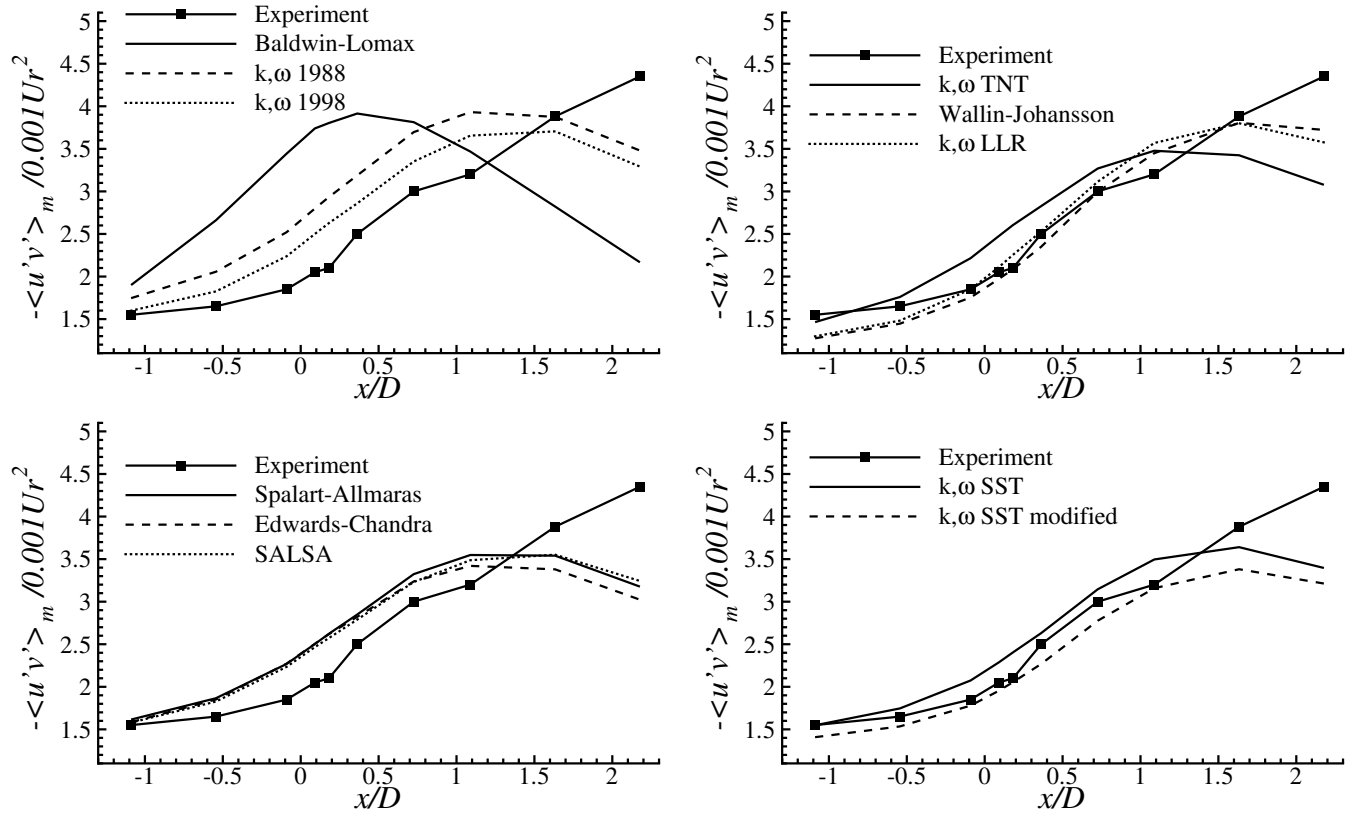

Fig. 6 Streamwise development of $-\overline{u'v'}_m$ for case CS0.

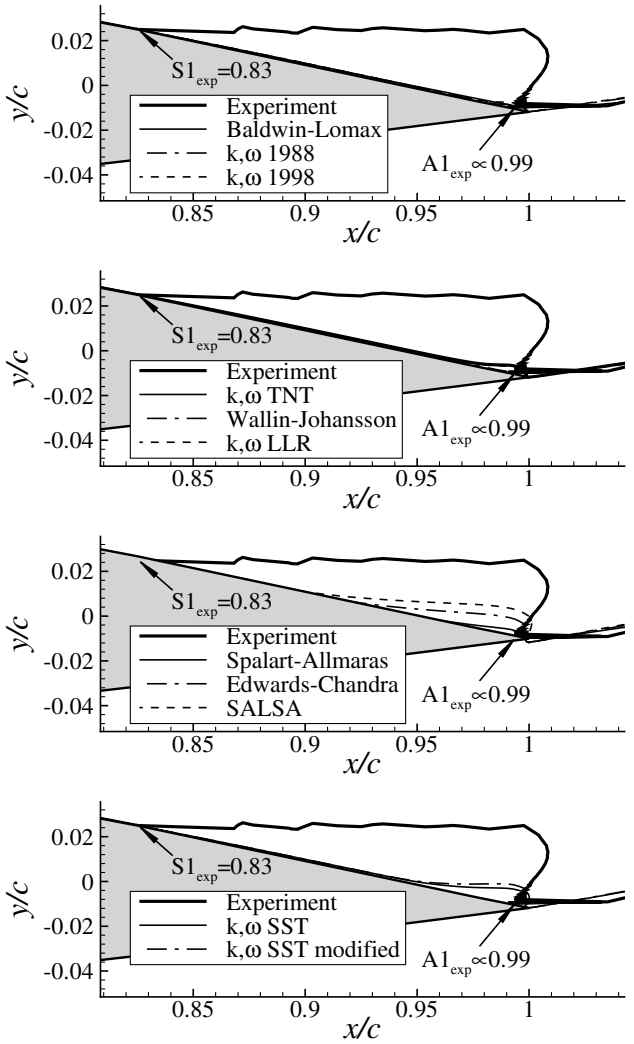

Fig. 7 Geometries of recirculation zones for airfoil A; dividing streamlines are shown.

Computations of this flow in the current study were performed on a grid with a classical C topology. A total of 512 cells in the wraparound direction with 384 cells placed on the airfoil surface were used. In the wall normal direction, 128 cells with 64 cells lying in the boundary layer were used. This gave $y^+ \leq 1$ everywhere. Far-field boundaries were located 18 chords away; characteristic boundary conditions in combination with vortex correction were prescribed at these boundaries. Grid points were clustered around the stagnation region, at the specified transition points, and in the trailing-edge separation zone. To mimic transition in the computation, productive source terms in the turbulence-transport equations were set to zero upstream of the transition points.

Evaluating streamlines at the trailing edge shows that the turbulence models predict recirculation zones that are smaller than the one found in the experiment (Fig. 7). This is in contrast to the results obtained for case CS0 where most models predict separation zones that are larger than the measured one. For the airfoil flow some, models, for example, both Wilcox models, do not yield a recirculation zone at all. The k, ω SST model and the SALSA model yield the largest separation zones.

All models compute c_p distributions that are above measured values at the rear part of the airfoil, i.e., for $x/c > 0.8$ (Fig. 8a). (Note that in the figure the direction of the c_p axis is reversed as is common practice for airfoil flows.) The plateau in the experimental pressure distribution encountered at the trailing edge on the upper surface of the airfoil is characteristic for separated flow regions. In the computational results, this pressure plateau is not reproduced.

Differences between computed pressure distributions are more pronounced at the suction peak than at the trailing edge with all models predicting a stronger suction peak than measured. This overprediction correlates with values predicted for the lift coefficient: The Baldwin–Lomax model, which produces the highest suction peak, yields the highest value for c_L, see Table 7. The k, ω SST models predict the lowest suction peak and the lowest lift. Yet, all models yield higher c_L than measured.

In Fig. 8b skin-friction distributions on the upper surface of the airfoil are compared for the region where experimental values are available ($0.3 \leq x/c \leq 0.99$). All models tend to predict $c_f = 0$ further downstream than seen in the experiment. However, the SALSA model and the one-equation model of Edwards and Chandra predict the position of $c_f = 0$ in very close agreement with measurements. These models also yield close agreement with the measured data for the almost zero level of c_f for $x/c \geq 0.87$.

Note that the exact separation location $S1_{exp}$ is not as clear for the airfoil flow as it is for the cylinder flow CS0. The position of $c_f = 0$ and the separation location inferred from the separating streamline differ by 0.04 chords in the experiment (compare Figs. 7 and 8). This is taken as an indication that the airfoil flow was not completely two-dimensional (in the sense of RANS) in the experiment.

All models produce a pitch-down moment (negative moment coefficient in Table 7) except the two k, ω SST models. They also yield the best agreement of c_p with the measurements at the suction peak and the trailing edge, see Fig. 8.

Concerning Reynolds shear stresses, all turbulence models except the Wallin–Johansson model yield predictions that are in fair agreement with experimental data up to $x/c = 0.6$ (Fig. 9). Downstream of this point, however, the models predict less Reynolds stress than measured. The strong increase of $-\overline{u'v'}_m$ seen in the experimental data for $x/c > 0.7$ is underpredicted except by the Baldwin–Lomax model. The Wallin–Johansson model yields the lowest values of $-\overline{u'v'}_m$ whereas the Baldwin–Lomax model and Menter's SST model predict the highest values.

Ratings of the models' performances for this flow case are given in Table 8. The only difference to the rating procedure applied for case CS0 is that instead of $c_{p\,\max}$ we use c_p at the stagnation point to normalize the averaged differences. According to the table, the SALSA models offers the closest agreement of computational results and experimental data.

Summary and Conclusions

Assessment of turbulence-model performance was pursued for the prediction of boundary-layer development with a strong adverse pressure gradient. For this purpose, a comparative study of 11 modern eddy-viscosity turbulence models was performed, with special regard to turbulent boundary-layer separation caused by an adverse pressure gradient. Four flow cases with increasing physical complexity were investigated. The cases consisted of a flat-plate boundary layer (case FPBL), a nonequilibrium boundary layer with a strong pressure gradient without separation (case BS0), a nonequilibrium boundary layer with pressure-induced separation (case CS0), and a separated airfoil flow (case AAA).

It was found that the agreement between computational and experimental results varied in particular for skin friction depending on the turbulence model used. In addition, predictive accuracy obtained with a given model for a given flow case varied between the variables evaluated. For example, good results were obtained with the SALSA model and the k, ω LLR model for surface pressure for the separated boundary-layer flow CS0, whereas modest results were obtained for skin friction.

For the separated airfoil flow, it was found that models that limit the eddy viscosity in boundary layers by applying the assumption of constant maximum value of the ratio between Reynolds shear stress and turbulent kinetic energy yielded better results than models not using this assumption. However, this finding does not hold for the two nonequilibrium boundary-layer cases BS0 and CS0. For example, the 1998 k, ω model by Wilcox does not build on this assumption, but it yields the best agreement of computational results with measurements for case BS0. Similarly, best results for case CS0

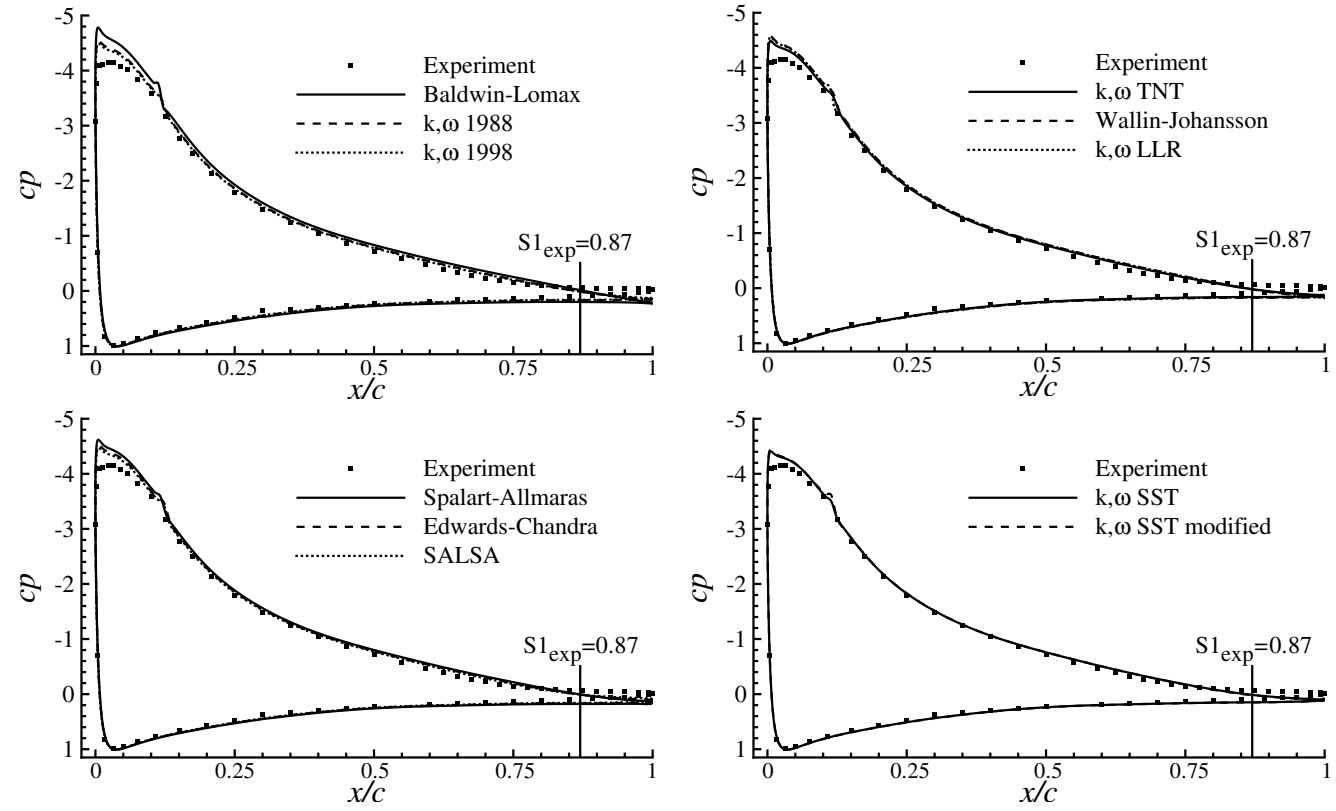

a) Pressure distrubtions

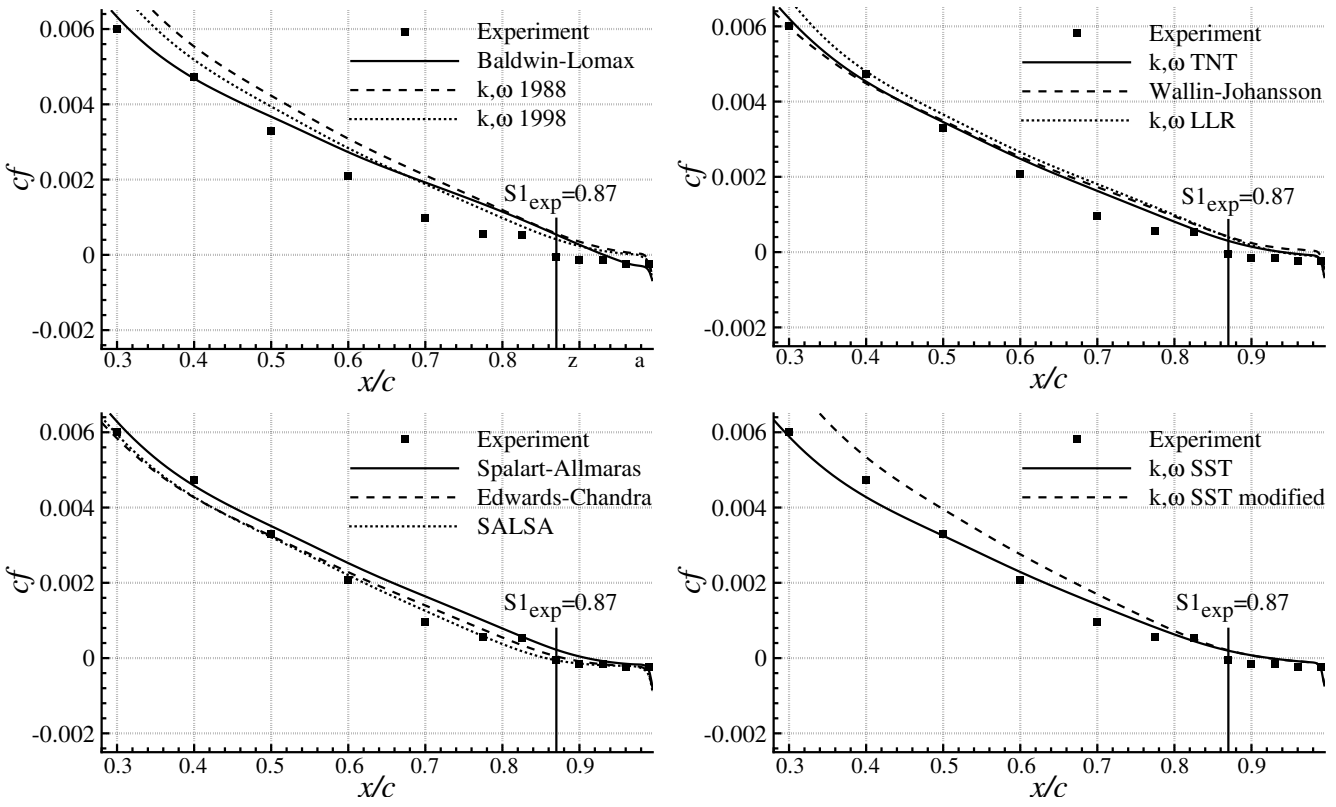

b) Skin-friction distributions

Fig. 8 Pressure and skin-friction distributions for separated airfoil flow (case AAA).

are obtained using the Wallin–Johansson model, which also does not employ this assumption.

For the flow cases with an adverse pressure gradient, models using transport equations for the eddy viscosity typically showed better predictive performance than the algebraic model. In addition, predictions of the one-equation models were found to be much closer to each other than those of the k, ω models.

Generally, computational results show less agreement with measurements for the separated airfoil flow than for the other flow cases investigated. We partly attribute this to uncertainties in the

Table 7 Aerodynamic coefficients for case AAA

	c_L	c_D	c_M
Experiment	1.56	0.021	(Not reported)
Baldwin–Lomax	1.73	0.0158	−0.0165
k, ω 1988	1.65	0.0175	−0.0044
k, ω 1998	1.63	0.0176	−0.0022
k, ω SST	1.60	0.0177	+0.0015
k, ω SST modified	1.60	0.0167	+0.0021
k, ω TNT	1.63	0.0166	−0.0014
k, ω LLR	1.65	0.0168	−0.0045
Wallin–Johansson	1.66	0.0153	−0.0044
Spalart–Allmaras	1.67	0.0166	−0.0088
Edwards–Chandra	1.64	0.0166	−0.0050
SALSA	1.62	0.0173	−0.0029

Table 8 Turbulence-model performance for airfoil A

Model	c_p	c_f	Separation zone	$-\overline{u'v'}_m$	$\sum$
SALSA	◯	2(++)	−−	− − −	1−
k, ω SST	◯	2(++)	−−	− − −	1−
Edwards–Chandra	2(−)	2(++)	−−	− − −	3−
k, ω SST modified	◯	◯	−−	− − −	5−
k, ω TNT	2(−)	2(+)	− − −	− − −	6−
Spalart–Allmaras	2(−−)	2(+)	− − −	− − −	8−
k, ω LLR	2(−)	◯	− − −	− − −	8−
Wallin–Johansson	2(−−)	2(+)	− − −	− − −	8−
k, ω 1998	2(−)	2(−)	− − −	− − −	10−
k, ω 1988	2(−)	2(−−)	− − −	− − −	12−
Baldwin–Lomax	2(− − −)	◯	− − −	− − −	12−

experimental data that are believed to be more significant for the airfoil flow than for the other flow cases. For example, measurements for c_L and c_D were performed in a different a wind tunnel than measurements for the other flow variables, e.g., u and $-\overline{u'v'}$. (Note, however, that differences between values measured in both wind tunnels are smaller than differences between computed and measured values.) In addition, there exist open questions about whether the flow around the airfoil was statistically steady and two-dimensional as assumed. For example, the separation location inferred from measured velocity profiles and the location where $c_f = 0$ differ by 0.04 chords. Nevertheless, we have based our rating on the agreement between measured and computed data because this flow case has been frequently used for the validation of turbulence models. However, it might prove to be necessary to revise this flow case for validation purposes of turbulence models for separated two-dimensional flows. For example, one could include the wind-tunnel walls in the computation and perform a three-dimensional simulation of the experimental setup to identify eventually existing three-dimensional flow features. This might, however, lead to other problems like, e.g., turbulence modeling in longitudinal corners.

The predictive performance of the turbulence models investigated is summarized in Table 9, which is of course subjective. The table is meant to serve as an attempt for recommending a turbulence model for a given flow class. For example, the 1998 k, ω model by Wilcox may be recommended for boundary-layer flows with a strong adverse pressure gradient without separation. However, many more computations of flows belonging to a given flow class must be performed before this kind of recommendation can be made on a thorough basis.

Flow classes in this context can be defined by the topology of the mean velocity field. For example, a flow class can comprise statistically steady and two-dimensional flows with a single recirculation zone. Following this line of reasoning, one can classify separated flows by the flow topology and investigate which turbulence model is best suited for computing which topological class. In this spirit, experiments may give more often conclusive information about what flow class is encountered. For example, two-dimensionality could be checked by balancing the momentum integral equation as done by Coles for the data in the 1968 AFOSR Stanford meeting or as done by Driver and Johnston for the cylinder flows. Similarly, statistical steadiness, e.g., no large-scale vortex shedding or flapping, could be verified by averaging measured data using different time periods (different number of samples). This would give hints about whether the flow under consideration can be,

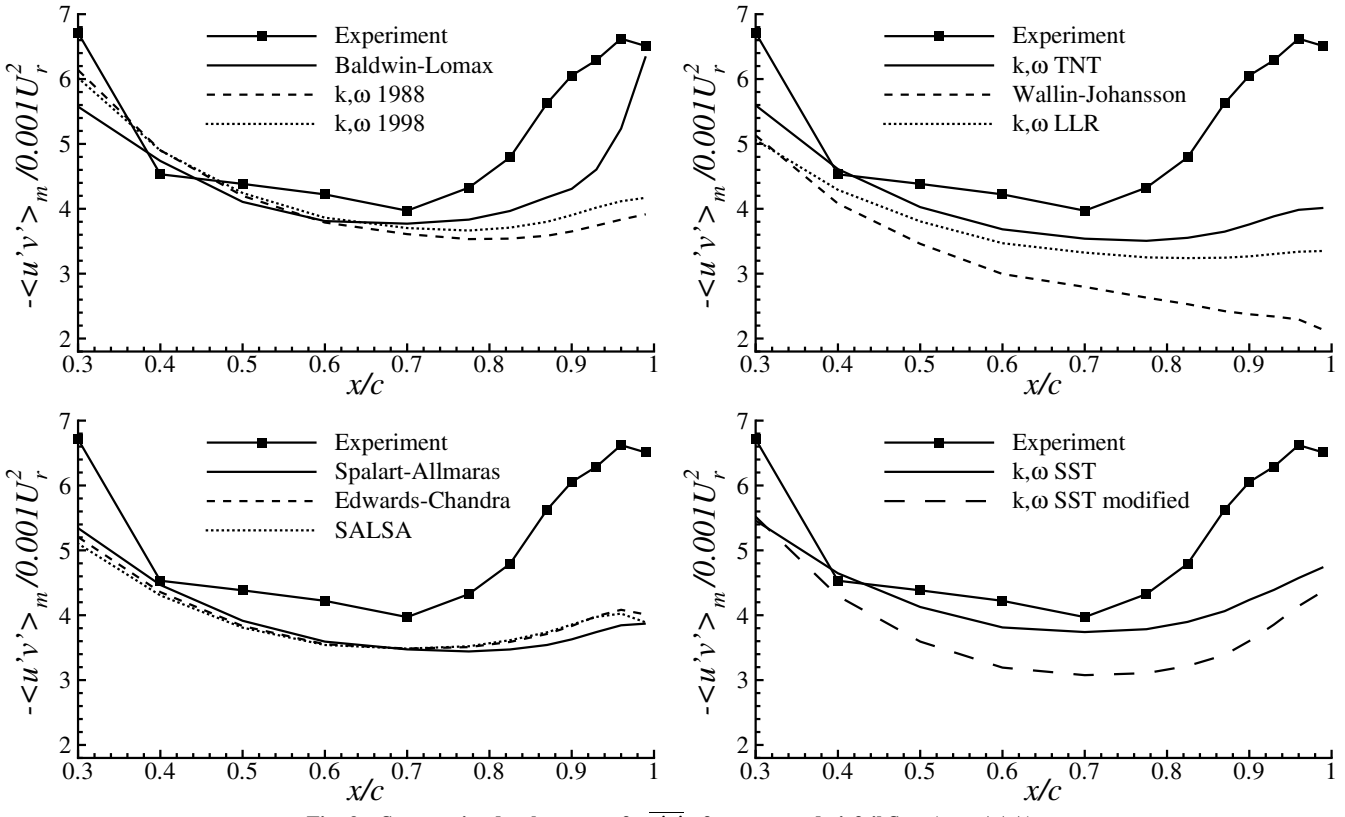

Fig. 9 Streamwise development of $-\overline{u'v'}_m$ for separated airfoil flow (case AAA).

Table 9 Summary of predictive performance of turbulence models investigated

Test case	FPBL flat plate	BS0 $\partial p/\partial x \geq 0$	CS0 $\frac{\partial p}{\partial x} \geq 0$ with separation	AAA separated airfoil flow
Good performance	k, ω SST modified k, ω TNT Spalart–Allmaras SALSA	k, ω 1998 Edwards–Chandra Spalart–Allmaras k, ω SST k, ω SST modified	Wallin–Johansson k, ω SST k, ω SST modified	——
Medium performance	k, ω LLR k, ω SST Baldwin–Lomax Edwards–Chandra k, ω 1998 Wallin–Johansson	SALSA Wallin–Johansson k, ω TNT k, ω LLR k, ω 1988 Baldwin–Lomax	k, ω 1998 k, ω LLR Edwards–Chandra SALSA Spalart–Allmaras k, ω 1988 k, ω TNT	SALSA k, ω SST Edwards–Chandra k, ω SST modified k, ω TNT
Poor performance	k, ω 1988	——	Baldwin–Lomax	Spalart–Allmaras k, ω LLR Wallin–Johansson k, ω 1998 k, ω 1988 Baldwin–Lomax

in principle, computed using a steady RANS method or whether unsteady computations have to be performed. It remains, however, an open question if statistically unsteady flows can be successfully predicted by RANS methods. We are pessimistic on this issue.

In addition, accurate experimental data about the location of transition and its extent are important because modeling of the transition region can be of crucial importance for the accurate computation of aerodynamic flows. Especially computations of airfoil flows, like the one considered in this work, depend heavily on accurate prescription of transition.

Acknowledgments

This work was supported by the Deutsche Forschungsgemeinschaft (Grants Hi 342/4-1 to 342/4-4). The authors gratefully acknowledge invaluable discussions with P. Bradshaw, W. Haase, and F. Menter. We also would like to thank the Deutsches Zentrum für Luft- und Raumfahrt in Braunschweig, Germany, for kindly providing the FLOWer code.

References

[1] Coles, D. E., and Hirst, E. A. (eds.), *Computation of Turbulent Boundary Layers—1968 AFOSR–IFP–Stanford Conference*, Vol. 2, Stanford University, Stanford, CA, 1969.

[2] Kline, S. J., Cantwell, B. J., and Lilley, G. M. (eds.), *Proceedings of the 1980-81 AFOSR–HTTM–Stanford Conference on Complex Turbulent Flows: Comparison of Computation and Experiment*, Stanford University, Stanford, CA, 1981.

[3] Bradshaw, P., Launder, B., and Lumley, J., "Collaborative Testing of Turbulence Models," *Journal of Fluids Engineering*, Vol. 118, No. 2, 1996, pp. 243–255.

[4] Haase, W., Bradsma, F., Leschziner, M., and Schwarmborn, D. (eds.), *EUROVAL: An European Initiative on Validation of CFD Codes*, Vol. 42, Notes on Numerical Fluid Mechanics, Vieweg, Brunswick, Germany, 1993.

[5] Haase, W., Chaput, E., Elsholz, F., Leschziner, M. A., and Müller, U. R. (eds.), *ECARP—European Computational Aerodynamics Research Project: Validation of CFD Codes and Assessment of Turbulence Models*, Vol. 58, Notes on Numerical Fluid Mechanics, Vieweg, Brunswick, Germany, 1997.

[6] Johnson, D. A., and King, L. S., "A Mathematically Simple Turbulence Closure Model for Attached and Separated Turbulent Boundary Layers," *AIAA Journal*, Vol. 23, No. 11, 1985, pp. 1684–1692.

[7] Vos, J. B., Rizzi, A., Darracq, D., and Hirschel, E. H., "Navier–Stokes Solvers in European Aircraft Design," *Progress in Aerospace Sciences*, Vol. 38, No. 8, 2002, pp. 601–697.

[8] Roache, P. J., *Verification and Validation in Computational Science and Engineering*, Hermosa, Alburquerque, NM, 1998.

[9] Kroll, N., Radespiel, R., and Rossow, C.-C., "Accurate and Efficient Flow Solver for 3D Applications on Structured Meshes," AGARD R-807, 1995.

[10] Aumann, P., Bartelheimer, W., Bleecke, H., Kuntz, M., Lieser, J., Monsen, E., Eisfeld, B., Fassbender, J., Heinrich, R., Kroll, N., Mauss, M., Raddatz, J., Reisch, U., Roll, B., and Schwarz, T., *FLOWer Installation and User Handbook*, Deutsches Zentrum für Luft- und Raumfahrt, Institut für Entwurfsaerodynamik, Brunswick, Germany, 2000.

[11] Kroll, N., Rossow, C.-C., Becker, K., and Thiele, F., "The MEGAFLOW Project," *Aerospace Science and Technology*, Vol. 4, No. 4, 2000, pp. 223–237.

[12] Fassbender, J., "Improved Robustness for Numerical Simulation of Turbulent Flows around Civil Transport Aircraft at Flight Reynolds Numbers," Deutsches Zentrum für Luft- und Raumfahrt, Rept. 2003-09, 2003.

[13] Baldwin, B. S., and Lomax, H., "Thin-Layer Approximation and Algebraic Model for Separated Flows," AIAA Paper 78-257, 1978.

[14] Wallin, S., and Johansson, A. V., "An Explicit Algebraic Reynolds Stress Model for Incompressible and Compressible Turbulent Flows," *Journal of Fluid Mechanics*, Vol. 403, Jan. 2000, pp. 89–132.

[15] Wilcox, D. C., *Turbulence Modeling for CFD*, 2nd ed., DCW Industries, La Cãnada, CA, 1998.

[16] Bardina, J. E., Huang, P. G., and Coakley, T. J., "Turbulence Modeling Validation," AIAA Paper 97-2121, 1997.

[17] Menter, F. R., "Performance of Popular Turbulence Models for Attached and Separated Adverse Pressure Gradient Flows," *AIAA Journal*, Vol. 30, No. 8, Aug. 1992, pp. 2066–2072.

[18] Rung, T., and Thiele, F., "Computational Modelling of Complex Boundary Layer Flows," *Proceedings of the 9th International Symposium on Transport Phenomena in Thermal-Fluid Engineering*, ISTP-9, 1996, pp. 321–326.

[19] Wilcox, D. C., "Reassessment of the Scale-Determining Equation for Advanced Turbulence Models," *AIAA Journal*, Vol. 26, No. 11, Nov. 1988, pp. 1299–1310.

[20] Kok, J. C., "Resolving the Dependence on Freestream Values for the k-ω Turbulence Model," *AIAA Journal*, Vol. 38, No. 7, July 2000, pp. 1292–1295.

[21] Shih, T.-H., Liou, W. W., Shabbir, A., Yang, Z., and Zhu, J., "A New k-ϵ Eddy Viscosity Model for High Reynolds Number Turbulent Flows," *Computers and Fluids*, Vol. 24, No. 3, 1995, pp. 227–238.

[22] Edwards, J. R., and Chandra, S., "Comparison of Eddy Viscosity-Transport Turbulence Models for Three-Dimensional, Shock-Separated Flows," *AIAA Journal*, Vol. 34, No. 4, 1996, pp. 756–763.

[23] Rung, T., Bunge, U., Schatz, M., and Thiele, F., "Restatement of the Spalart–Allmaras Eddy-Viscosity Model in a Strain-Adaptive Formulation," *AIAA Journal*, Vol. 41, No. 7, 2003, pp. 1396–1399.

[24] Spalart, P. R., and Allmaras, S. R., "A One-Equation Turbulence Model for Aerodynamic Flows," AIAA Paper 92-0439, Jan. 1992.

[25] Bradshaw, P., Ferriss, D. H., and Atwell, N. P., "Calculation of Boundary-Layer Development Using the Turbulent Energy Equation," *Journal of Fluid Mechanics*, Vol. 28, May 1967, pp. 593–616.

[26] Menter, F. R., "Two-Equation Eddy-Viscosity Turbulence Models for Engineering Applications," *AIAA Journal*, Vol. 32, No. 8, Aug. 1994, pp. 1598–1605.

[27] Menter, F. R., "Influence of Freestream Values on k-ω Turbulence Model Predictions," *AIAA Journal*, Vol. 30, No. 6, June 1992, pp. 1657–1659.
[28] DeGraaff, D. B., and Eaton, J. K., "Reynolds-Number Scaling of the Flat-Plate Turbulent Boundary Layer," *Journal of Fluid Mechanics*, Vol. 422, Nov. 2000, pp. 319–346.
[29] Driver, D. M., and Johnston, P., "Experimental Study of a Three-Dimensional Shear-Driven Turbulent Boundary Layer with Streamwise Adverse Pressure Gradient," NASA TM 102211, May 1990.
[30] Celić, A., "Performance of Modern Eddy-Viscosity Turbulence Models," Ph.D. Thesis, Universität Stuttgart, 2004.
[31] Chaput, E., "Aerospatiale-A Airfoil," *ECARP—European Computational Aerodynamics Research Project: Validation of CFD Codes and Assessment of Turbulence Models*, edited by W. Haase, E. Chaput, F. Elsholz, M. A. Leschziner, and U. R. Müller, Vol. 58, Notes on Numerical Fluid Mechanics, Vieweg, Brunswick, Germany, 1997, pp. 327–346.
[32] Davidson, L., Cokljat, D., Fröhlich, J., Leschziner, M. A., Mellen, C., and Rodi, W. (eds.), *Large Eddy Simulation of Flow Around a Lifting Airfoil: Results of the Project LESFOIL Supported by the European Union 1998–2001*, Vol. 83, Notes on Numerical Fluid Mechanics and Multidisciplinary Design, Springer–Verlag, Berlin, 2003.

S. Aggarwal
Associate Editor